THE JOURNAL OF NAVIGATION (2006), **59**, 105–117. © The Royal Institute of Navigation
doi:10.1017/S037346330500353X Printed in the United Kingdom

A Highly Accurate and Computationally Efficient Method for Predicting RAIM Holes

Shaojun Feng and Washington Y. Ochieng

(*Imperial College London*)
(Email: w.ochieng@imperial.ac.uk)

David Walsh and Rigas Ioannides

(*University of Leeds*)

Receiver Autonomous Integrity Monitoring (RAIM) is a method implemented within the receiver to protect users against satellite navigation system failures. For a receiver to execute a RAIM calculation, two conditions must be met: a minimum number of satellites and adequate satellite geometry. The non-existence of the minimum number of satellites (five) is referred to as a *RAIM hole*. Current regional and global RAIM availability studies use spatial (grid-based) and temporal sampling intervals driven by a trade-off between accuracy and computation workload. The implication of minimising computational load is that accuracy is compromised and potential RAIM holes remain un-sampled, with potential risk to safety. This paper proposes a direct and computationally efficient method (as opposed to the grid-based search approach) to predict RAIM holes. The method is based on the precise computation of satellite coverage (footprint) boundaries, the intersection points and analysis of the topology of the regions of intersection. Test results show that the proposed method is highly accurate and requires minimal computational load compared to the current approach.

KEY WORDS

1. Integrity Monitoring 2. GNSS 3. RAIM hole

1. INTRODUCTION. Receiver Autonomous Integrity Monitoring (RAIM) is a receiver-based scheme to provide timely and valid warnings to users if a Global Navigation Satellite System (GNSS) is not able to meet the required navigation performance (RNP). RAIM algorithms are based on statistical consistency checks using redundant measurements. Consistency checks require that at least five satellites are visible, while in the case of Failure Detection and Exclusion (FDE), at least six visible satellites are required. A RAIM hole occurs for the period of time that there are insufficient navigation satellites in view to provide an integrity check at a given location. It is defined to be the time during which less than five GNSS satellites are in view above a mask angle of 7·5 degrees [1]. RAIM holes are the result

of information shortage causing the RAIM algorithm to be unable to perform its function. Similarly, we can define the FDE hole to be the time that less than six GNSS satellites are in view above a mask angle of 7·5 degrees.

Theoretically, RAIM holes are predictable because they are the result of the relative motion of the navigation satellites with respect to the Earth. For a single point on the Earth, it is straightforward to predict the RAIM holes by assessing the number of visible satellites in the time domain. For an aircraft trajectory, the prediction is based on trajectory space-time points, with an aircraft only at one space point on the trajectory at any given time. In the case of performance assessment over an area, the prediction of RAIM holes is more complicated because of both the spatial and temporal variations. The requirement to sample all geometries to provide a high accuracy performance assessment could result in a very large number of space-time points. The method commonly used is to overlay a grid over an area of interest and to search at the nodes over time. Example spatial and temporal intervals that have been used in RAIM availability assessment include: 5 degrees and 5 minutes [2], 3 degrees and 5 minutes [3, 4], while Eurocontrol employs 0·25 degrees and 2·5 minutes in the AUGUR software [5]. These sampling intervals are relatively large and are therefore susceptible to RAIM holes. Hence, if the spatial and temporal intervals are too large, then some RAIM holes could pass undetected if they lie either between the spatial or temporal sampling points. However, smaller intervals result in a large number of sample points requiring increased computational resources. The grid-based search method is therefore always dependent upon a trade-off between accuracy and computational load.

This paper proposes a pure computation method to predict RAIM holes. The exact coverage boundaries and intersection points of the boundaries of each satellite are calculated by extrapolating from the Earth's spherical model to the ellipsoidal model. A topology analysis of the regions formed by the intersection of the satellite coverage boundaries is then carried out. The paper is organised as follows. Section 2 presents the problem investigated. The algorithms and procedure are presented in Sections 3 and 4 respectively. Test results are presented in Section 5 followed by a discussion in Section 6. The paper is concluded in Section 7.

2. PROBLEM DESCRIPTION.

Looking down towards the Earth, each navigation satellite covers a certain area of the Earth's surface. For a given mask angle, the coverage region on the Earth is a closed surface with a coverage boundary. The points that comprise the region are individually characterised as either lying entirely within the region or its boundary. Thus, this set of points denoted by R can be divided into two subsets R_I and R_B, where R_I is the subset of points in the interior of a region and R_B is the subset of points on its boundary. This can be written as:

$$R = [R_I \; R_B] \tag{1}$$

For a modelled surface, such as the surface of a sphere or ellipsoid, a region can be completely described by the boundary R_B because the interior of the region R_I can be determined by the surface model. Hence, the boundary can be exploited positively in a RAIM hole prediction process.

https://doi.org/10.1017/S037346330500353X Published online by Cambridge University Press

The overlap of n satellite coverage areas (or footprints) forms a region where there must be n satellites in view. This region can be expressed as:

$$R^N = [R_I^N \; R_B^N] = \bigcap_{i=1}^{n} R^i \tag{2}$$

The region R^N is a closed surface, bounded by the segments of m ($2 \leqslant m \leqslant n$) coverage boundaries. Figure 1 shows the intersection region for $m = 3$. Each segment has a start point and an end point. These points are an exact subset of boundary intersection points. Therefore, the coverage boundary of each satellite and the boundary intersection points form the boundary of the region R_B^N.

The determination of the coverage boundaries and the intersection points is not straightforward. The coverage boundary, in fact, is the intersection of two surfaces, one is the Earth surface, and the other is a cone-like surface. There are several methods to compute the intersection of two surfaces [6]. Generally, a physical surface can be represented by meshes of bi-cubic patches. The procedure for finding surface intersections is decomposed into three distinct phases: the mesh grid hunting phase, the tracking phase, and the sorting phase. The hunting phase locates discrete starting points at each mesh required for the curve-tracking operation. The tracking phase creates strings of points lying on the intersection. In the sorting phase the point strings are ordered and separated into segments or loops. Figure 2 shows the difference between mesh hunting points and grid-based search points. It also demonstrates how the grid-based search method oversimplifies the problem, which may lead to a RAIM hole not being detected even if it covers several grid areas.

The problem investigated here has an additional complication compared to the conventional surface intersection determination methods in that the two surfaces concerned are correlated by the mask angle. Although the ellipsoid model is a more accurate approximation of the Earth than the spherical model, with the constraints of a constant mask angle, the coverage boundary does not always describe the exact shape of an ellipse.

3. THE PINPOINT COMPUTATION ALGORITHM.

The basic idea of determining RAIM holes is to find the precise coverage boundary of each satellite for a given mask angle (i.e. 7·5 degrees), and then to determine all the intersection points. Possible RAIM holes can then be determined by a topology analysis of the intersecting regions.

3.1. *Determination of satellite coverage boundary*. The Earth is initially considered to be a sphere, and therefore the region between the satellite and its footprint boundary on the sphere has the exact shape of a cone. This enables an initial (approximate) satellite coverage boundary to be calculated. This is followed by an iterative transformation from the spherical model to the ellipsoidal model of the Earth, generating a precise satellite coverage boundary. For the spherical model, the basic relationships between satellite coverage and various angles are shown in Figure 3a. The nadir, central and elevation angles are denoted by α, β, and θ respectively. s is the slant distance, r_{sat} is the distance between the satellite and the Earth's centre, r_e is the radius of the Earth, and T is the orthogonal angle between the radius of the sphere and a plane tangent to the sphere surface at point P.

https://doi.org/10.1017/S037346330500353X Published online by Cambridge University Press

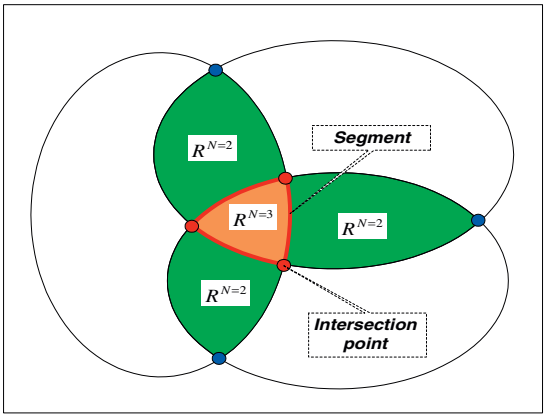

Figure 1. Intersection of coverage and boundary segments.

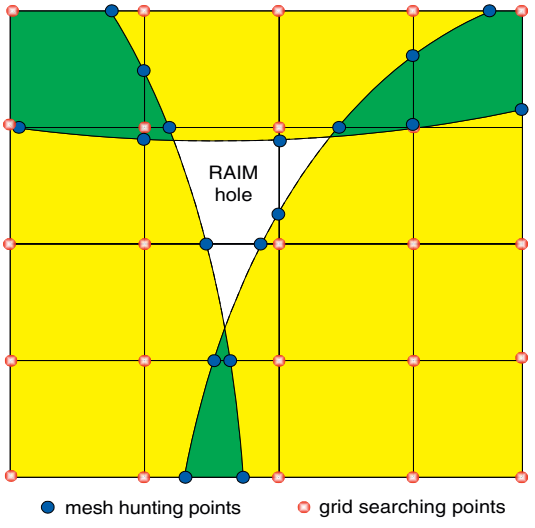

Figure 2. Mesh hunting points and grid search points.

The fundamental relationships between these angles and distances are given by:

$$\alpha = \arcsin\left(\frac{r_e}{r_{sat}}\cos(\theta)\right) \tag{3}$$

$$\alpha + \beta + \theta = 90^\circ \tag{4}$$

$$\beta = \arcsin\left(\frac{r_{sat}}{r_e}\sin(\alpha)\right) - \alpha \tag{5}$$

The position of a satellite can be determined from the satellite's almanac, broadcast ephemeris, or precise ephemeris. Furthermore, the satellite foot point on the Earth's surface and the distance between the satellite and the Earth's centre r_{sat} can be

https://doi.org/10.1017/S037346330500353X Published online by Cambridge University Press

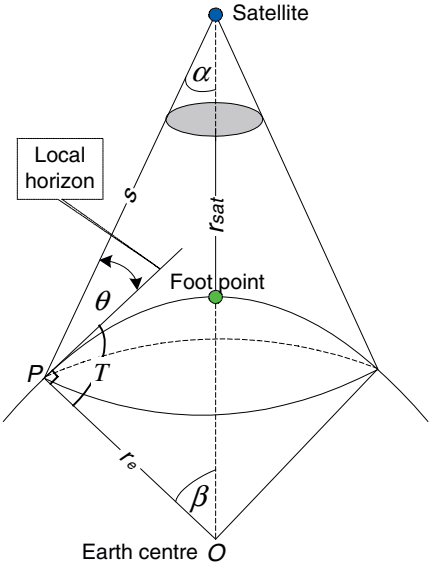

Figure 3a. Relationships between satellite coverage and various angles.

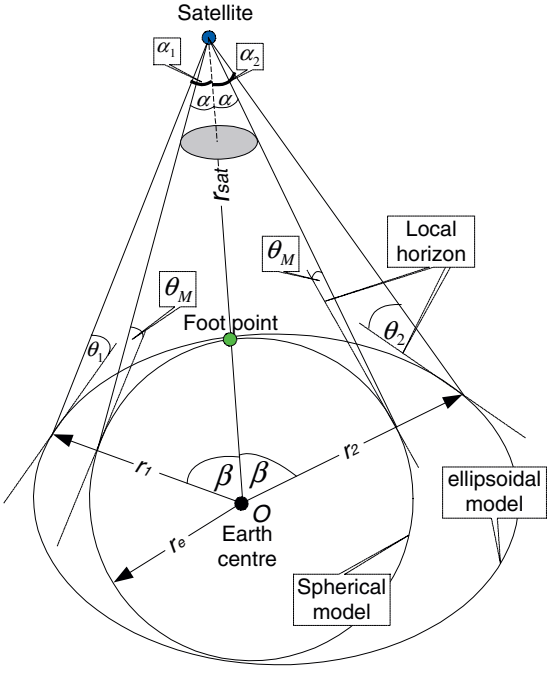

Figure 3b. Differences between spherical and ellipsoidal model.

calculated. Since the elevation angle θ and the radius of the Earth r_e are known, the nadir angle α, and the central angle β can be calculated directly using equations (3–5). The coverage boundary is a small circle with its centre point at the

https://doi.org/10.1017/S037346330500353X Published online by Cambridge University Press

satellite foot point and a radius equal to the central angle β in units of angular arc length.

For a given mask angle θ_M, the central angle β_0 can be calculated directly using expression (3) and (5). The position of a point on the small circle can therefore be calculated from the position of satellite foot point, central angle, and a given direction by:

$$\phi_0 = \sin^{-1}(\sin\phi_f \cos\beta_0 + \cos\phi_f \sin\beta_0 \cos\psi) \tag{6}$$

$$\lambda_0 = \mathrm{mod}\left(\left(\lambda_f - \tan^{-1}\left(\frac{\sin\psi \sin\beta_0 \cos\phi_f}{\cos\beta_0 - \sin\phi_0 \cos\phi_f}\right) + \pi\right), 2\pi\right) - \pi \tag{7}$$

where ϕ_0, λ_0 are the latitude and longitude of the point on the boundary in the spherical model. ϕ_f, λ_f are the latitude and longitude of the satellite foot point. ψ is the azimuth from satellite foot point to the point on boundary, and $\pi = 3{\cdot}1415926535898$.

In the ellipsoidal model, the coverage boundary is not necessarily a small circle and the central angle β is no longer a constant but a function of (ϕ_f, λ_f), ψ and θ_M. To transform to the ellipsoidal model, the coordinates (ϕ_0, λ_0) of the point above are used directly to calculate the elevation angle by assuming the point is on the surface of the ellipsoid. The resulting error between the calculated elevation angle and the mask angle is due to the differences in the radii and local horizons. Figure 3b demonstrates the scenario where the local horizons and the radii are different, $r_1 \neq r_e$, $r_2 \neq r_e$, $r_1 \neq r_2$, and $\theta_1 \neq \theta_M$, $\theta_2 \neq \theta_M$, $\theta_1 \neq \theta_2$ even with the same central angle β. The difference between the calculated elevation angle and mask angle together with central angle β_0, can be taken as initial values for an iterative transformation from the spherical model to the ellipsoidal model. The elevation angle algorithm plays the role of transformation because the final decision whether a satellite is visible is based on the calculated elevation angle. The purpose is to find the points on the surface of ellipsoid whose elevation angles equal the mask angle.

For a point on the boundary, the error in the elevation angle can be expressed as:

$$\Delta\theta_i = \theta_i - \theta_M \tag{8}$$

where $\Delta\theta_i$, θ_i denote the errors in the elevation angle and the calculated elevation angle respectively in the $(i-1)^{th}$ iteration. The corrected central angle can be expressed as:

$$\beta_i = \beta_{i-1} + \Delta\theta_{i-1} \tag{9}$$

where β_i is the central angle for the i^{th} iteration for the precise position of the point on coverage boundary.

The central angle β_i is fed back to expressions (6) and (7) by replacing β_0. The point position (ϕ_i, λ_i) and corresponding θ_i can then be calculated. The iteration process stops when $\Delta\theta_i$ is small enough to meet a specified accuracy requirement. After a few iterations, the precise ellipsoidal coordinates of the point on coverage boundary can be determined. What should be highlighted is that the angle T in Figure 3a is

https://doi.org/10.1017/S037346330500353X Published online by Cambridge University Press

not necessarily an orthogonal angle and expression (4) does not hold in the iterative process.

3.2. *Determination of boundary intersection points.* The intersection points are determined using the same procedure as for the coverage boundary determination. The initial intersection points are based on the Earth's spherical model. In a second step, they are extrapolated to the ellipsoidal model using the same iterative method as described in section 3·1.

Consider two satellites shown in Figure 4, with foot points B and C on the Earth surface, and the centre of the Earth at O. If the two boundaries intersect, generally there are two intersection points (D and D'). Tangency of two coverage boundaries is a special case where points D and D' coincide with each other. The central angles β_B and β_C can be calculated from the mask angle. For the spherical model, β_B, β'_B, β_C and β'_C have the same value ($\beta_B=\beta'_B=\beta_C=\beta'_C$) for the same mask angle value. The great circle distance (d) can also be determined from the location of the two foot points B and C. According to the laws of spherical triangles,

$$\angle D = \arccos\left(\frac{\cos(d) - \cos(\beta_B)\cos(\beta_C)}{\sin(\beta_B)\sin(\beta_C)}\right) \tag{10}$$

$$\angle B = \arcsin\left(\frac{\sin(\angle D)\sin(\beta_B)}{\sin(d)}\right) \tag{11}$$

where $\angle D$, $\angle B$ are the angles in the spherical triangle shown in Figure 4.

The azimuth from point B to C, ψ_{BC} can be calculated based on the location of points B and C; and the azimuths from point B to D and D', i.e. ψ_{BD} and $\psi_{BD'}$, can be calculated from:

$$\psi_{BD} = \psi_{BC} + \angle B \tag{12}$$

$$\psi_{BD'} = \psi_{BC} - \angle B \tag{13}$$

From point B, along the directions given by ψ_{BD} and $\psi_{BD'}$, and distance equal to β_C, the location of points D and D' can be found by expressions (6) and (7) and the following iteration process.

Checking the elevation angle at the intersection points D (D'), we find that it is not the same as the mask angle. This is due to the same reason as in the coverage boundary determination. However, we take these points as the initial location for the iteration from the Earth's spherical model to the ellipsoidal model. At either point D or D', there are two elevation angles to the satellites B and C. The error in these two elevation angles can be expressed as:

$$\begin{aligned} \Delta\theta_B^i &= \theta_B^i - \theta_M \\ \Delta\theta_C^i &= \theta_C^i - \theta_M \end{aligned} \tag{14}$$

where $\Delta\theta_B^i$ and $\Delta\theta_C^i$ are the error in the elevation angle for satellites B and C respectively. θ_B^i and θ_C^i are the actual elevation angles with the initial value with respect to β_B, β_C determined from the spherical model. θ_M is the mask angle. The

https://doi.org/10.1017/S037346330500353X Published online by Cambridge University Press

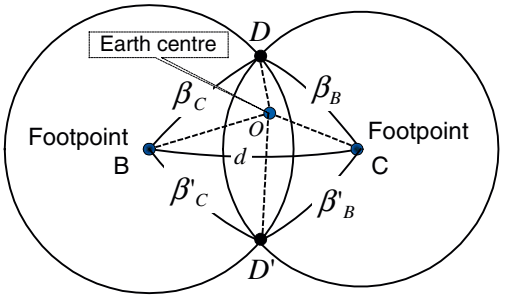

Figure 4. Intersection of two satellite coverage borders.

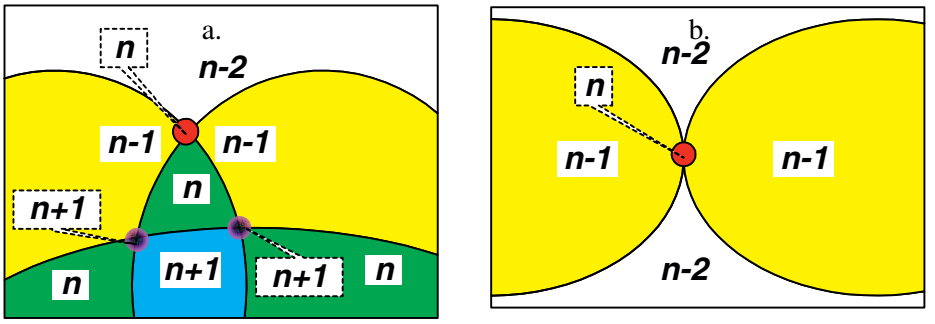

Figure 5. (a) Topology of two boundary intersection regions. (b) Topology of regions around the tangent point.

corrected central angles can then be expressed as:

$$\begin{aligned}\beta_B^i &= \beta_B^{i-1} + \Delta\theta_B^{i-1} \\ \beta_C^i &= \beta_C^{i-1} + \Delta\theta_C^{i-1}\end{aligned} \tag{15}$$

where β_B^i and β_C^i are the central angles at the i^{th} iteration. The initial values β_B^0 and β_C^0 ($i=0$) are taken as the central angles (β_B and β_C) determined from the spherical Earth model. The central angles β_B^i and β_C^i are then fed back to expression (10) and (11) by replacing β_B and β_C. The iteration process stops when $\Delta\theta_i$ is small enough to meet a specified accuracy requirement. After a few iterations, the precise intersection points can be determined. What should be highlighted is that the central angles β_B^i and β_C^i (and other combinations) do not necessarily have the same value in the iterative process.

3.3. *Topology of intersecting regions.* A RAIM hole does not necessarily occur around the intersection points. Whether there is a RAIM hole depends on the number of visible satellites at the intersection points and the topology of the intersection regions around them.

There are four regions around each intersection point of two satellite coverage boundaries. If an intersection point falls within the footprint of n satellites, the intersection region formed by the two satellites and delimited by nearby footprints

https://doi.org/10.1017/S037346330500353X Published online by Cambridge University Press

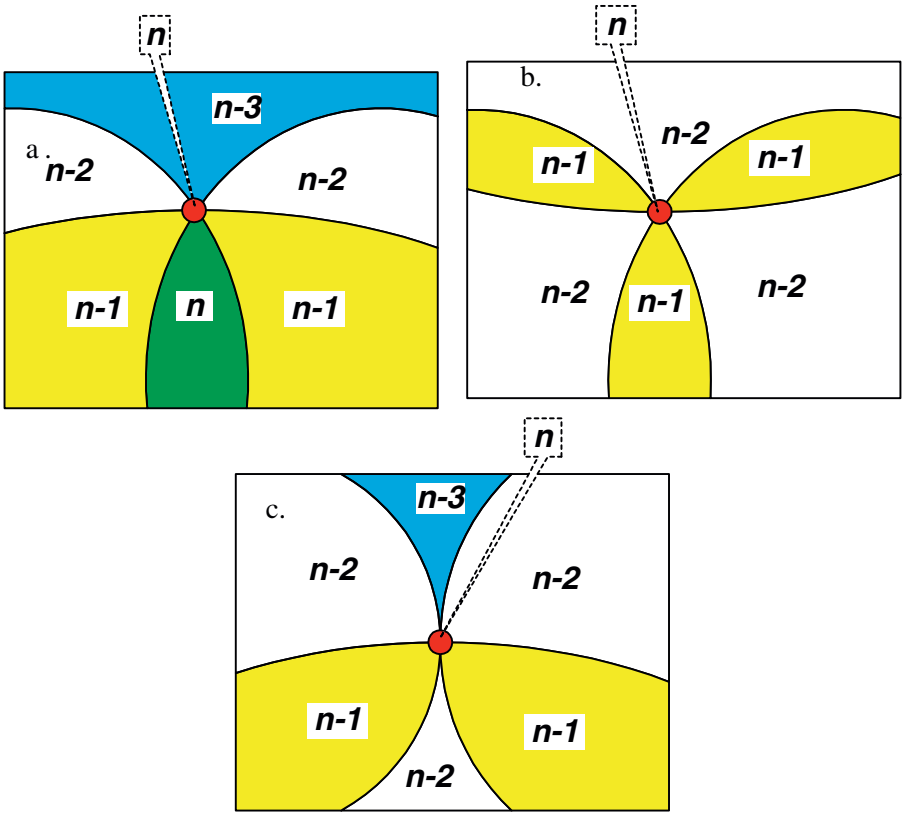

Figure 6. (a) and (b) Topology of three boundary intersection regions. (c) Topology of regions around tangent and intersection point.

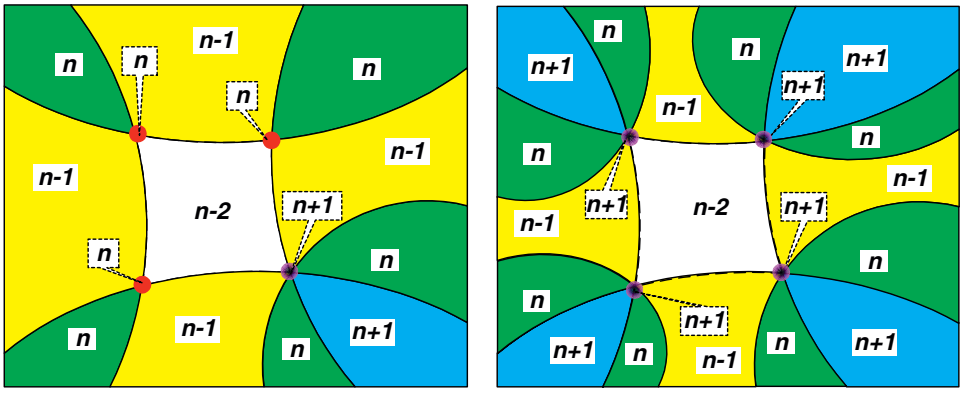

Figure 7. (a) and (b). Topology of multiple regions.

has n satellites in view. The two adjacent regions to the intersection region are areas with $(n-1)$ satellites in view. The region on the opposite side to the intersection region is the area with $(n-2)$ satellites in view. The number of visible satellites on

https://doi.org/10.1017/S037346330500353X Published online by Cambridge University Press

the coverage boundary is the larger number of visible satellites of the two adjacent regions. Figure 5a shows the topology of a two boundary of intersection delimited by a nearby footprint. One special case is the existence of a tangent between two boundaries where only the tangent point has the maximum number of visible satellites. Figure 5b shows the topology of regions around the tangent point between two boundaries.

Figures 6a, 6b, and 6c show the topology of regions for different scenarios considering an intersection point in the three boundary case. Figures 7a and 7b show the topology of multiple regions.

If an intersection point has six satellites ($n=6$) in view, according to the topology, there must be at least one region with only four satellites in view, i.e. a RAIM hole, and two regions with only five satellites in view, i.e. an FDE hole. In some special cases, such as shown in Figures 6a and 6c, RAIM holes could occur even with more than six satellites in view at an intersection point. However, because both the Earth and the satellite coverage area on the Earth are closed surfaces, there must be at least one other intersection point with six satellites in view (i.e. two boundaries intersect) because the intersection region is also a closed surface as shown in Figure 7a. The extreme case rarely occurs where a RAIM hole is formed by all the intersection points of the three boundaries and segments of adjacent boundaries as shown in Figure 7b.

4. RAIM HOLE DETERMINATION PROCEDURE.

Given the algorithms described in the preceding sections, the process for the determination of RAIM holes consists of a number of steps as given below.

- Determination of the positions of all satellites
- Determination of the foot points of all satellites in ellipsoidal model
- Determination of the rough intersection points of all satellites in ellipsoidal model
- Iterative determination of the precise intersection points of all satellites
- Checking the visible satellite number at each intersection point. If the visible satellite number is less than six ($n \leqslant 6$) record the location of the intersection point and the identification (ID) numbers of the satellites involved.
- Sorting the recorded intersection points to form a closed region from the recorded satellite IDs.
- Iterate to determine the segments of the boundaries from the recorded satellite IDs and the intersection points which form the closed region.

As described in section 2, a region on a modelled surface can be completely described by the regional boundary. Therefore, the region enclosed by the segments of boundaries determines the precise location of the RAIM hole.

5. RESULTS.

A global RAIM hole calculation was carried out to verify the pinpoint algorithm. The optimised 24 Global Positioning System (GPS) constellation [4] was used to determine the positions of satellites. The Earth's ellipsoidal model was taken as WGS-84.

The RAIM holes at 403500th, 403700th and 403900th seconds of week are shown in Figures 8a, 8b, and 8c respectively. The RAIM holes and the coloured areas in the diagrams are bounded by the satellite footprint boundaries. The numbers beside the intersection points are the numbers of visible satellites at those points. These figures also show how the shape and size of RAIM holes change over time. A further example is shown in Figure 9 where the RAIM hole covers part of the land.

6. DISCUSSION. The proposed algorithm is able to find the satellite coverage boundaries and intersection points with high precision. The elevation angle errors relative to the mask angle at the determined points are at the level of 1×10^{-4} degrees after one iteration, and 1×10^{-10} degrees after six iterations. With this accuracy, unless three or more satellite boundaries intersect at exactly one point, (see Figures 6a, 6c, 7a and 7b the probability of this happening is significantly low), the probability of detecting the closed region bounded by the intersecting boundaries is extremely high. Even in the rare cases where more than two footprint boundaries intersect at the same point, any potential RAIM holes are still detectable because at least one other intersection point will have six satellites in view. If the algorithm finds that the intersection points with six satellites in view are not able to form a closed region, a very short temporal shift of say, 0·001 seconds is sufficient for the satellites to move to reveal a RAIM hole.

The accuracy of the results depends on the accuracy of the satellite and 3-D user position information and the actual height of the user above the ellipsoidal model surface. The computation workload of the proposed method is significantly smaller than that of the grid-based search method. For example, considering two satellite foot print boundary intersections for a 24 satellite constellation at a time, generates 276 combinations, equivalent to a maximum number of intersection points equal to 552. Considering six iterations for both β_B and β_C, there are a maximum of 6624 points. In addition, there are 100 points for each regional segment, which need six iterations. Assuming there are 5 segments, an additional 3000 points are obtained. Combining these, a total calculation of 9624 points is needed, which for example, is less than the number of points in a $2{\cdot}5^\circ \times 2{\cdot}5^\circ$ global spatial grid. Furthermore, the accuracy of the method presented in this paper is much higher than the grid-based search method, even with a $0{\cdot}25^\circ \times 0{\cdot}25^\circ$ grid resolution.

7. CONCLUSION. In this paper, a method to compute precise satellite coverage boundaries and the intersection points determined by a given mask angle was developed. The RAIM holes were found in two ways: one by using the direct computation instead of the grid-based search method, and the other by using bounded regions to express RAIM holes instead of the points-based approximation. The advantages of the method presented in this paper are accuracy with less computational load. There is no possibility of even the smallest RAIM holes passing undetected. The method can be used for GPS, or Galileo integrity performance assessments, and can also be used for RAIM hole predictions especially for regional (such as General Aviation) or global applications.

https://doi.org/10.1017/S037346330500353X Published online by Cambridge University Press

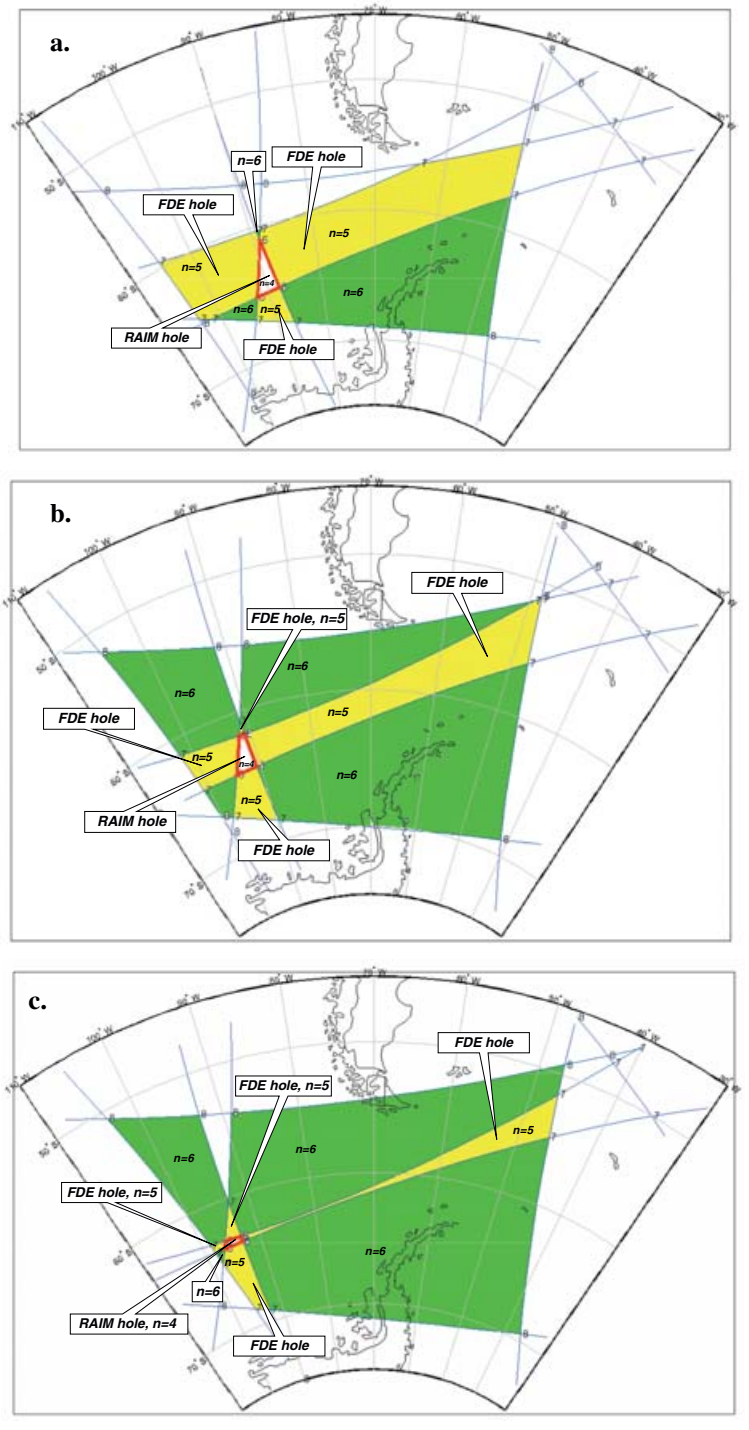

Figure 8. (a). RAIM hole at the 403500th second. (b). RAIM hole at the 403700th second. (c). RAIM hole at the 403900th second.

https://doi.org/10.1017/S037346330500353X Published online by Cambridge University Press

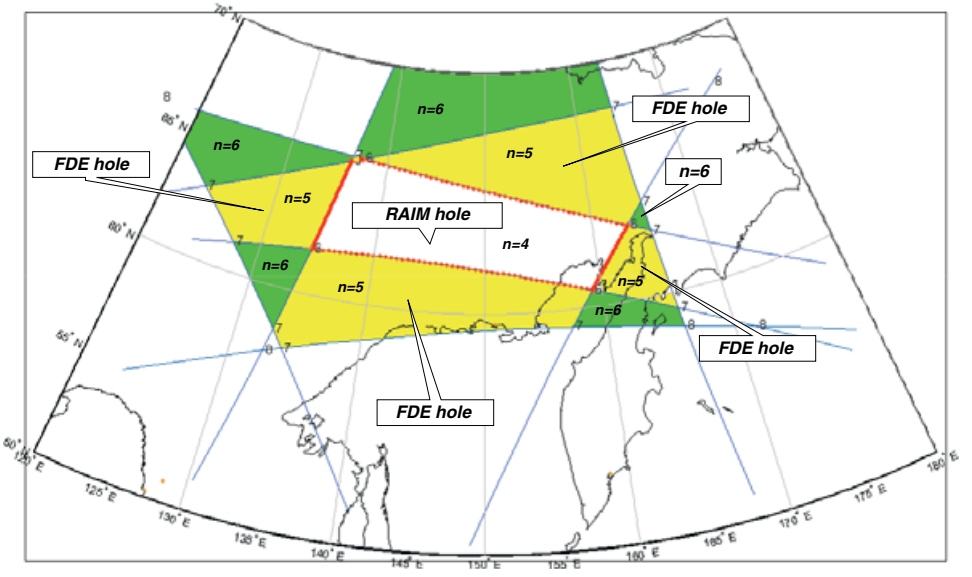

Figure 9. RAIM hole at the 604700th second.

REFERENCES

[1] Air force space command capstone requirements document for global position, velocity, and time determination capability. http://www.navcen.uscg.gov/pubs/gps/crd/crd.pdf, July, 1997.
[2] Ochieng, W. Y., Sheridan, K. F., Sauer, K., and Han, X. (2002). An assessment of the RAIM performance of a combined Galileo/GPS navigation system using the marginally detectable errors (MDE) algorithm. *GPS Solution*. **5**, 3, 42–51.
[3] TSO-C129a (1996), Airborne supplemental navigation equipment using the global positioning system (GPS), Department of Transportation Federal Aviation Administration Aircraft Certification Service, Washington, DC, February, 1996
[4] RTCA/DO-229B (1999), Minimum operational performance standards for global positioning system/wide area augmentation system airborne equipment. October, 1999
[5] *http://augur.ecacnav.com/augurHelp.html*
[6] Mortenson, M. E. (1997), *Geometric modeling*, Wiley.

https://doi.org/10.1017/S037346330500353X Published online by Cambridge University Press